Liquid flow in surface-nanostructured channels studied by molecular dynamics simulation

Bing-Yang Cao,* Min Chen, and Zeng-Yuan Guo
Department of Engineering Mechanics, Tsinghua University, Beijing 100084, China
(Received 27 July 2006; published 29 December 2006)

Molecular dynamics simulations have been carried out to investigate the fluid wetting and flow in nanochannels whose surfaces are structured by an array of nanoscale triangular modules. We find that the surface nanostructures have a dual effect on the boundary slip and friction of the liquid nanoflow. On the one hand, the nanostructures can enhance the surface hydrophilicity for a hydrophilic liquid-solid interaction, and can increase the hydrophobicity for a hydrophobic interaction due to a nanoscale lotus effect. In particular, the nanostructured surface may show superhydrophobicity and lead to the large velocity slip of the liquid flow. On the other hand, simultaneously, the nanostructures distort the nanoscale streamlines of the liquid flow near the channel surfaces and block the nanoflow directly, which decreases the apparent slip length equivalently. The dual effect of the nanostructures on the surface wettability and the hydrodynamic disturbance results in a nonmonotonic dependence of the slip length on the nanostructure size. The simulations imply that the surface nanostructures can be applied to control the friction of liquid micro- and nanoflows.

DOI: 10.1103/PhysRevE.74.066311 PACS number(s): 47.61.−k, 47.11.Mn, 68.08.Bc, 47.85.lb

I. INTRODUCTION

Liquid flow in micro- and nanoscale channels is widely used in recently advanced MEMS and NEMS (micro/nano-electromechanical systems), micro-total-analytical systems (μTAS) and lab-on-a-biochip [1–3]. Surface effects substantially dominate the flow due to the high surface-to-volume ratio in micro- and nano-fluidic devices [4,5]. The liquid flow in micro- and nanochannels becomes much more difficult than that in macroscale channels, which greatly bottlenecks the performance, miniaturization, and economy improvement of the micro- and nanodevices. However, there are very few demonstrated methods for reducing the friction of the liquid micro- and nanoflow.

Quite a few literatures published during the past decade, which have been reviewed in Ref. [6], show that liquids flowing over a solid surface actually do slip and the no-slip boundary condition for the liquid flow is merely an approximation at macroscale-length scale. The conventional no-slip and slip boundary conditions (BC) of a Poiseuille flow are schematically shown in Fig. 1, in which u_s is the slip velocity defined as the velocity difference between the solid and the liquid adjacent to the wall, L_s is the slip length defined by Navier's model $u_s = L_s(\partial u_x/\partial z)_{\text{wall}}$, and H is the characteristic length of the flow system. The friction coefficient of the Poiseuille flow, which characterizes the flow drag, can be written as

$$f = \frac{48}{\text{Re}} \frac{1}{1 + 6\dfrac{L_s}{H}}, \tag{1}$$

in which Re is Reynolds number [7]. It indicates that the boundary slip always decreases the friction mainly depending on the ratio of the slip length and the characteristic length of the flow system. The slip effect becomes very important in the micro- and nanoscale flow as the characteristic length decreases. In other words, the friction decrease requires the slip increase.

The velocity slip of liquid flow at a solid surface has been measured experimentally [8–16] (for a recent review see Ref. [17]) and simulated by the molecular dynamics (MD) method [18–25]. The factors dominating the liquid-solid slip in the experimental measurements often include surface wettability, surface roughness, shear rate, gas films, nanobubles, and even unknown ones. Most of them have hitherto remained unanswered about how to influence the liquid-solid slip phenomena, except for the liquid-solid wettability. The surface hydrophobicity has been confirmed to enhance the velocity slip. It is not difficult to accept that a hydrophobic surface indicates a weak interaction between liquid and solid and an easier sliding for the fluid molecules across the solid. For example, in the experimental measurements carried out by Tretheway and Meinhart [11], an apparent slip length was measured about 1 μm for water flowing in an octadecyltrichlorosilane-coated microchannel where the contact angle is about 120°. The MD simulation presents a powerful tool for studying the mechanism of the liquid-solid BC at the atomic level since the liquid-surface interaction can be

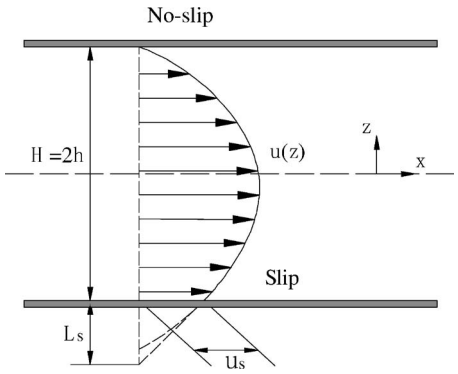

FIG. 1. Schematic diagram of boundary conditions of Poiseuille flow.

*Corresponding author. FAX: 86-10-6278-1610; Email address: caoby@tsinghua.edu.cn

adjusted at one's pleasure. The boundary behaviors from stick to slip have been observed with from strong to weak liquid-solid interactions. For the liquid flowing past a hydrophilic surface, the liquid adjacent to a wall is often stuck to the solid due to the strong surface force and there is not velocity slip at the liquid-solid boundary. However, for the liquid flow at a hydrophobic surface, much larger slip has been observed in the existing MD studies [18–25]. The obtained slip length by MD simulations exceeds 30 molecular diameters for a liquid-solid contact angle of 140° in Barrat and Bocquet's work [21].

Originally inspired by the unique property of the superhydrophobicity of lotus leaves [26] and water strider legs [27], which is specially called the "lotus effect," we believe that surface microscale structures may enhance the surface hydrophobicity and then increase the velocity slip of the liquid flow at a structured surface. Bonaccurso and co-workers [28] were the first to find that the degree of liquid slip increased with nanoscale surface roughness in their hydrodynamics drainage force measurements though no specific mechanism was proclaimed. Large slip lengths of 20–100 μm were recently measured for liquid flows over superhydrophobic surfaces, which were designed and fabricated with different micro/nanoscale structures according to the lotus effect idea [29–34]. The lotus effect on the nanoscale for nanodroplets on structured [35] or patterned [36] surfaces was also demonstrated by MD simulations. The door to reducing the micro- and nanoflow drag seems to be being opened. However, we should note that there are also conflicting results, which indicated that surface structures or roughness would suppress the velocity slip by experimental studies [9,12], MD calculations [37,38], and theoretical analyses [39–41].

The effects of the surface structures on the micro- and nanoflow boundary conditions may be more complex due to different mechanisms [42–44]. The wetting of the lotus leaves with micro- and nanoscale structures is often in a heterogeneous state, which means that there must be patches of air beneath the structure gaps. However, the liquid flows in engineering situations may actually be homogeneous. In order to investigate how the liquid wets a nanostructured surface and how the surface nanostructures affect the liquid flows, the molecular dynamics simulation method is applied to study liquid flow in nanochannels whose surfaces are nanostructured by an array of triangular modules. In Sec. II, we describe the simulation details. In Sec. III, our simulation results and discussion are presented. Finally, we draw conclusions in Sec. IV.

II. SIMULATION DETAILS

Molecular dynamics simulations on liquid-vapor-solid wetting and Poiseuille flow phenomena are carried out. The systems are constructed as shown schematically in Fig. 2. Two parallel plates form a channel with the distance $H=10.2$ nm. The y-direction length of all our simulation systems is $L_y=1.96$ nm. The walls are taken to be platinum or its modeling solid. In the nanochannel is the fluid argon. A periodic boundary condition is used along the x and y direction, i.e., directions parallel to the solid plates. We build the

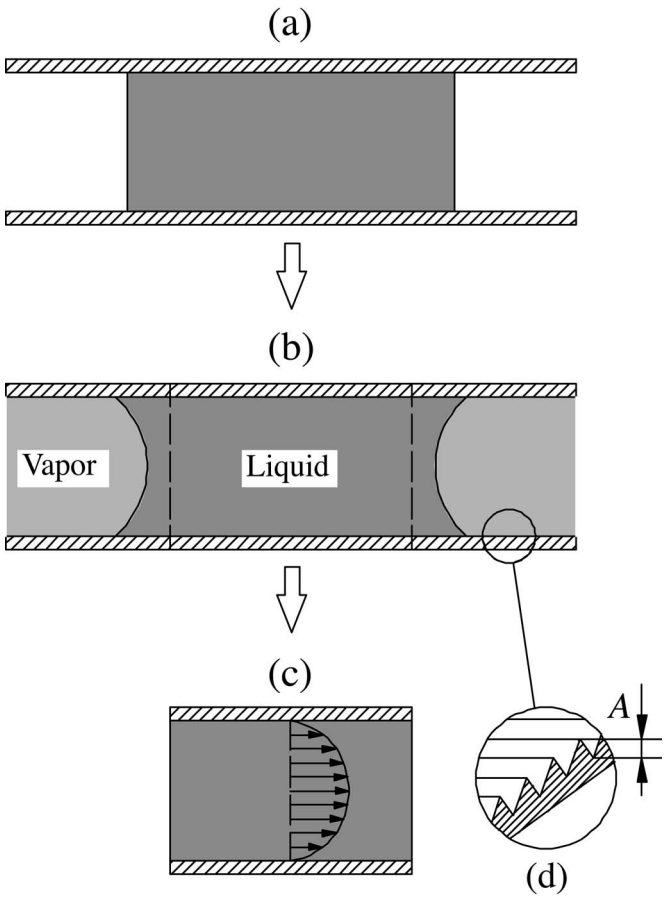

FIG. 2. The simulation system and its constructing procedures. We construct the simulation ensembles through three steps: initial configuration (a), liquid-vapor coexistence in the nanochannel (b), and channel Poiseuille flow (c). In (d) is the three-dimensional view of the surface nanostructures with a size of A.

simulation systems through the following procedures. As an initial condition illustrated in Fig. 1(a), a cubic argon droplet with the saturation density at a certain temperature is placed in the middle of the channel. Then, we start to run our program to drive the system to reach a steady thermodynamic state with liquid-vapor coexistence as shown in Fig. 2(b). Thus, the wettability between the fluid and the surface can be obtained by measuring the contact angle of the liquid-vapor meniscus. Finally, the middle section containing no vapor is segmented out only along the x direction to form a flow MD configuration as shown in Fig. 2(c). A Poiseuille flow is simulated to study the boundary slip. The channel surfaces are structured by an array of triangle modules, as shown in Fig. 2(d), with sizes A of 0.39, 0.78, 1.18, 1.57, and 1.96 nm, respectively. The liquid flow in smooth nanochannels, i.e., $A=0$, is also simulated as a benchmark case. It should be pointed out that the x direction system length must be integral times of the surface nanostructure size in our MD simulations in order to apply the periodic boundary condition along the x direction. In our vapor-liquid coexistence simulations, the x-direction system length is about $L_x=58.76-59.54$ nm. In the liquid-flow calculations, the x-direction length is about $L_x=18.80-21.94$ nm.

It is important to note the difference between the present MD work and the existing literatures in some main aspects: (1) The contact angles and the boundary slips are simultaneously calculated; (2) we set up more realistic solid materials and nanostructure geometries rather than varying the liquid-solid interaction parameters; (3) the liquid-vapor coexistence step leads to constant thermodynamics states for all our simulation cases.

The present simulations form nonequilibrium systems in which the fluid (liquid and vapor) is confined by the solid walls. In our vapor-liquid coexistence simulations, the calculated systems contain 8900 argon fluid molecules and 6000 platinum solid atoms. In the liquid nanoflow calculations, the simulation systems often have about 5200 fluid molecules and 2000 wall atoms. The particle number calculated in the present work is large enough for calculating the contact angle of the wetting meniscus [35,36,45] and the characteristics of nanoflow boundary conditions [18–25,37,38].

In order to maintain a realistic fluid-solid boundary condition, we build atomic structure walls based on Einstein theory that the wall atoms vibrate around their face-centered-cubic (fcc) lattice sites with the Einstein frequency tethered by a harmonic spring of stiffness [46]

$$E = \frac{16\pi^4 k^2 m^2 \theta^2}{h^2}, \tag{2}$$

where k is the Boltzmann constant, h is the Planck constant, m is the mass of a wall atom, and θ=180 K is the Einstein temperature of platinum. The wall is controlled at a constant temperature T=120 K for each simulation by a velocity rescaling method expressed as

$$v_i = v_{it}\sqrt{\frac{T}{T_t}}. \tag{3}$$

Particle interactions with each other are via a Lennard-Jones (LJ) 12-6 potential in the form

$$\phi(r) = 4\varepsilon\left[\left(\frac{\sigma}{r}\right)^{12} - \left(\frac{\sigma}{r}\right)^{6}\right], \tag{4}$$

where r is the intermolecular distance, ε and σ are, respectively, the energy and molecular diameter parameters. For the argon-argon interaction, $\sigma = 3.405 \times 10^{-10}$ m is chosen as a length unit and $\varepsilon = 1.67 \times 10^{-21}$ J is applied as an energy unit. We use $\sigma_{AP} = 3.085 \times 10^{-10}$ m and $\varepsilon_{AP} = 0.894 \times 10^{-21}$ J for the argon-platinum interaction [47]. For the potential interaction between the fluids (argon) and the solids, the LJ energy parameter is varied as

$$\varepsilon_{AS} = c\varepsilon_{AP}, \tag{5}$$

where the potential coefficient c determines the liquid-wall interface tension. The wettability of a smooth surface depends on the coefficient c as well. With a large value of the potential coefficient c, the surface often shows hydrophilicity, which is called a hydrophilic interaction between liquid and solid. A little value usually makes the surface to be hydrophobic, which is then called a hydrophobic liquid-solid interaction.

The Poiseuille flow is induced by subjecting the fluid molecules to an external driving field $g_x = 1-5 \times 10^{10}$ m/s^2 and is locally fully developed (LFD) to be laminar with Reynolds numbers in the range of 5–50. The velocity shear rate on the nanoflow boundary is much smaller than the critical value $\dot{\gamma}_c \sim (m\sigma_{AP}^2/\varepsilon_{AP})^{-1/2}$, and thus the boundary slip length should be independent of the driving field in our simulations [48]. In the case of the planar Poiseuille flow of a Newtonian fluid under constant external force, the macroscopic hydrodynamics gives a parabolic solution of the Navier-Stokes (NS) equation. Considering the slip boundary condition, the velocity profile of a LFD flow may be written as

$$u_x = \frac{\rho g_x}{2\mu}(h^2 - z^2) + u_s, \tag{6}$$

in which z is the distance from the middle of the channel, ρ is the density of the liquids, μ is the dynamical viscosity, and u_s is the slip velocity at the liquid-solid boundary. Running averages of the velocity in 40 x-oriented bins of equal width covering the whole channel, we can calculate the velocity profile of the LFD Poiseuille flow. The slip velocity can easily be obtained through analyzing the velocity profile. According to the Navier boundary condition, the slip length can be calculated by extrapolating the velocity profiles from the position in the fluid to where the velocity would vanish. In our simulations, the slip length L_s is computed by

$$L_s = u_s \Big/ \left(\frac{du_x}{dz}\right)_{|z|=h}. \tag{7}$$

The molecules move according to Newton's second law. The equations of motion are integrated using a leapfrog Verlet algorithm with a time step of dt=2.15 ps [49]. To reduce the time-consuming part of the calculation of interparticle interactions, we mainly take two measures: (a) A typical potential cutoff of $r_{cut} = 2.5\sigma$ is shifted; (b) the cell-linked list method is adopted. The fluid (liquid and vapor) system is also maintained at the constant temperature T=120 K for each simulation by a Langevin thermostat method in the y and z directions [50]. The motion equation of the ith molecule in the y and z directions is

$$m\ddot{r}_i = \sum_{j \neq i} \frac{\partial \phi_{LJ}}{\partial r_i} - m\Gamma \dot{r}_i + \eta_i, \tag{8}$$

where $m = 6.63 \times 10^{-26}$ kg is the mass of an argon atom, Γ is a friction constant determining the rate of heat exchange between the simulation system and a heat reservoir, and η_i is a Gaussian-distributed random force.

A steady thermodynamic state of liquid-vapor coexistence often requires an equilibrium time of about 500,000 time steps in our simulations. Dividing the system into 300 $\times$300 cells projecting to the xz plane, we then average the density profiles of the simulation system for 1 000 000 steps in order to measure the contact angle. Reaching a fully developed state for the simulated Poiseuille flow cost another 500,000 time steps. Then the velocity profiles can be collected through an averaging method over 1 000 000 time steps.

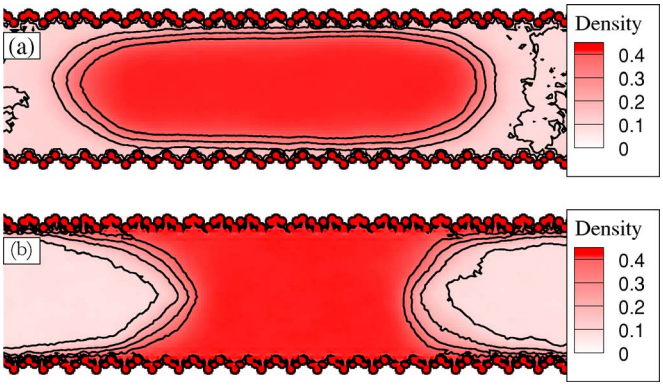

FIG. 3. (Color online) Density contours of the liquid-vapor coexistence in the nanostructured channels with (a) $A=0.78$ nm, $c=0.4$; and (b) $A=0.78$ nm, $c=1.0$. The fluid density in the legends is rescaled by the unit σ^{-3}. The zigzag contours in the up and down sides of the figures are due to the solid surface and the induced ordering of the fluid.

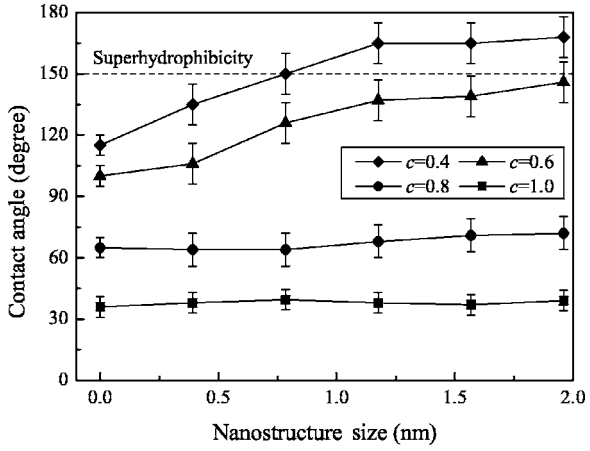

FIG. 4. Effect of the surface nanostructures on the contact angle. $A=0$ means the channel surface is smooth. A contact angle more than 150° is referred to as superhydrophobicity.

III. RESULTS AND DISCUSSION

The fluid-surface wettability can be obtained from the spreading state of the argon droplet in the nanochannel. We first simulate the droplet spreading in a smooth channel. The calculated contact angle of argon in the smooth platinum channel, i.e., $c=1.0$, is 36°, which agrees well with the result of 34° of an argon nanodroplet over a platinum substrate by MD simulation in Ref. [35]. Neglecting the atomic structure of the solid interface, the contact angle can theoretically be given by [51]

$$\theta_s \approx \cos^{-1}\left(2c\frac{\varepsilon_{AP}}{\varepsilon}-1\right). \tag{9}$$

The formula gives $\theta_s \approx 38°$, which confirms our MD simulations. By varying the energy parameter c, we can change the liquid-solid wettability from hydrophilicity to hydrophobicity. The simulated contact angles with $c=0.8$, 0.6, and 0.4 are, respectively, $\theta_s=65°$, 100°, and 115°. Thus, the fluid-solid interaction is hydrophilic for $c=1.0$ and 0.8, but is hydrophobic for $c=0.6$ and 0.4.

Taking the nanochannel with surface nanostructures of $A=0.78$ nm as a case, the wetting states of the liquid pillars in the channels are obtained through our liquid-vapor coexistence simulations as shown in Fig. 3. We can find that the wetting models of fluid over the nanostructured surface are quite different for the hydrophilic and hydrophobic liquid-solid interactions. For the hydrophobic liquid-solid interaction with $c=0.4$ as shown in Fig. 3(a), the liquid droplet partially suspends over peaks of the surface nanostructures. The liquid cannot fully fill the nanostructure gaps and the density of the liquids near the surfaces is lowered. Such a wetting is exactly heterogeneous, and the contact angle of the nanostructured surface can be described by the Cassie model [52]

$$\theta_n = \cos^{-1}(\psi\cos\theta_s + \psi - 1), \tag{10}$$

where ψ is the area fraction of the liquids contacting with the solids. The heterogeneous wetting makes ψ less than one, and the contact angle is increased. This is exactly a nanoscale lotus effect. The contact angle with $A=0.78$ nm and $c=0.4$ is about 150°, which is much larger than that of the smooth surface. However, for the hydrophilic liquid-solid interaction with $c=1.0$ as shown in Fig. 3(b), the fluid can wet the surface nanostructures completely. The crystallized liquid layers with a higher density adjacent to the nanostructured solid walls are observed [18]. The wetting becomes homogeneous. The contact angle of such a nanostructured surface can be expressed by the Wenzel model [53,54]

$$\theta_n = \cos^{-1}\left(s\cos\theta_s - \frac{f}{\sigma_{LV}}\right), \tag{11}$$

in which s is the ratio of the nanostructured surface area and its projection area, f is the hysteresis tension, and σ_{LV} is the liquid-vapor interface tension. For the triangular nanostructures, s is equal to 2.0. The contact angle with $A=0.78$ nm and $c=1.0$ is about 39.5°. It is because of the hysteresis tension why the contact angle variation affected by the nanostructures compared with the smooth surface is not very large for the hydrophilic liquid-wall interaction.

The contact angles affected by the surface nanostructures are shown in Fig. 4. For the hydrophobic liquid-wall interaction with $c=0.4$ and $c=0.6$, the contact angle increases with the increasing nanostructure size. The surface with larger nanostructures can even show superhydrophobicity, i.e., $\theta_n > 150°$. The hydrophobicity enhancement by the surface nanostructures can be interpreted by the Cassie theory mentioned above. However, the contact angle seems not to be affected by the surface nanostructures for the hydrophilic interaction. In fact, we measure the advanced contact angle in our simulations. From Eq. (11) of the Wenzel theory, the hysteresis tension may approximately counteract the nanostructure wettability effect.

We now turn our attention to the boundary conditions between the liquid and the nanostructured surface. Figure 5 shows the velocity profiles in the x direction averaged by our MD simulations. We can find that all the curves of the velocity profiles appear quadratic in the middle of the channels.

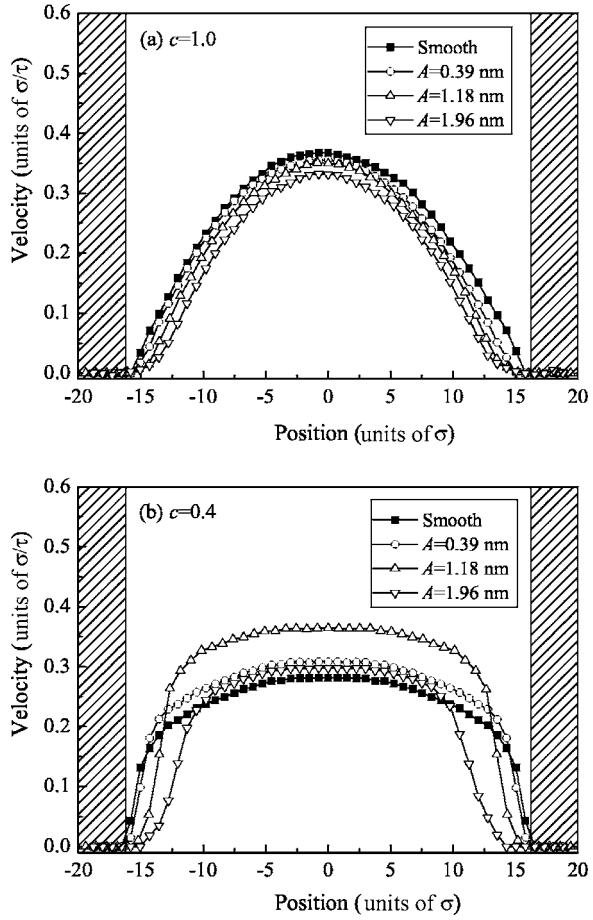

FIG. 5. Effect of surface nanostructures on the velocity profiles with (a) $c=1.0$ and (b) $c=0.4$. The hatching panes represent the solid surfaces of the nanochannels. We set the channel boundaries at the half height, i.e., $A/2$ of the surface nanogeometries in all our calculations.

This is really the case predicted by Eq. (6). It indicates that the mainstream regime of a liquid nanoflow at the present simulation scale obeys the continuum mechanics described by the NS equation. For the hydrophilic liquid-solid interaction with $c=1.0$, the effect of the surface nanostructures on the velocity profiles is shown in Fig. 5(a). The velocity smoothly decreases to about zero near the surfaces for the liquid flow over a smooth surface. It indicates that the slip velocity of the liquid flow at the boundaries is very small. With the increasing nanostructure size, the macroscopic velocity of the liquids adjacent to the channel surfaces decreases. The mean velocity across the nanochannels is decreased by the nanostructures, and the boundary velocity slip is consequently reduced. For a larger nanostructure, e.g., $A=1.96$ nm, the velocity gradient near the walls is clearly reduced by the surface nanogeometries, which indicates an apparent block to the liquid nanoflow. In this case, the slip velocity extracted from Eq. (6) becomes negative, which is often defined as a negative slip [18,41]. In Fig. 5(b), we present the effect of the surface nanostructures on the velocity profiles with $c=0.4$, where the liquid-wall interaction is hydrophobic. A large velocity slip of the liquid flow over the smooth channel surface can be observed. With the surface

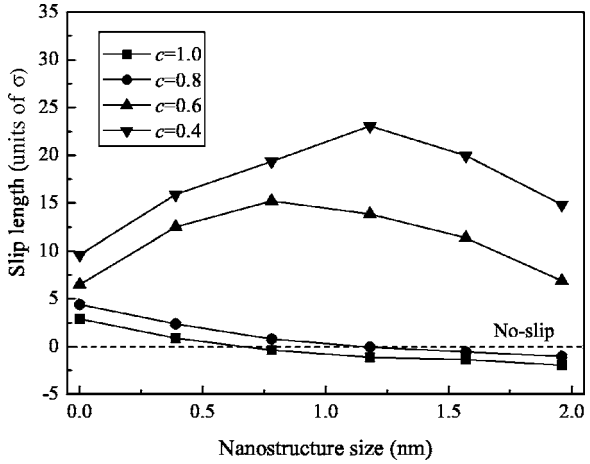

FIG. 6. Dependence of the slip length on the nanostructures and the liquid-wall interaction. Positive (negative) slip length indicates the extrapolated velocity vanishes outside (inside) the nanochannel. The zero slip length denotes the no-slip boundary condition.

nanostructures, the velocity gradients of the liquid flow near the channel boundary become larger than that near smooth walls, which indicates that the boundary slip is enhanced by the nanostructures and takes place inside the liquids adjacent to the surfaces. Over a hydrophobic surface with nanostructures, the fluid density is lowered. As a result, the momentum exchange between the fluid and the wall should be reduced. The near-surface fluid becomes very rarefied in the nanochannels and causes large velocity slips like in the rarefied gas dynamics. It has been demonstrated above that the surface wettability is greatly enhanced by the nanostructures and reaches superhydrophobicity of a contact angle 170° with $A=1.96$ nm. The boundary slip of liquid flow in the nanochannel with $A=1.96$ nm is less than those with $A=1.18$ nm and $A=0.39$ nm, though the surface hydrophobicity increases with the nanostructure size. In most of previous literatures on the boundary slip of liquid flows in smooth nanochannels [18–25], a weaker liquid-solid interaction, i.e., a more hydrophobic wettability, was often found to lead to a larger slip length. However, we find that the boundary slip in the present work is not a monotonic increasing function along with the nanostructure size, i.e., the increasing surface hydrophobicity, with the surface nanostructure effect. It may indicate that the velocity slip does not merely depend on the channel surface wettability.

Figure 6 summarizes the slip length dependence on the surface nanostructures and the liquid-wall interaction coefficient. For $c=1.0$ and $c=0.8$, the liquid-wall interaction is hydrophilic, and the slip length is decreased by the nanostructures monotonically. The slip length is about $-1.92\,\sigma$ for $c=1.0$ and $A=1.96$ nm, which increase the nanoflow friction by 62.3%. For the hydrophobic liquid-wall interaction with $c=0.6$ and $c=0.4$, however, the slip length varies along with the nanostructure sizes nonmonotonically. The slip is increased by the nanostructures with less size and is then decreased by larger size nanostructures. In the present simulations, the maximum slip length is about 23.1σ (7.9 nm) with $c=0.4$ and $A=1.18$ nm, which can even reduce the nanoflow friction by 82.2%. The $A=1.96$ nm nanostructure

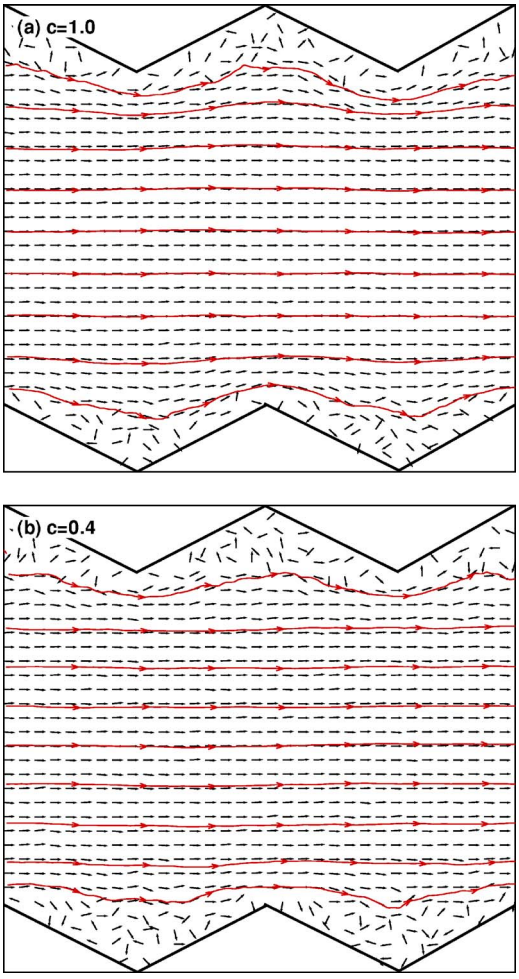

FIG. 7. (Color online) Streamlines of the liquid flows in nanostructured nanochannels with (a) $c=1.0$ and (b) $c=0.4$. The velocity fields are in the x-z plane.

leads to a 14.8σ slip length, which then decreases the friction by 74.7%. We may also see that very large surface structures will always decrease the boundary slip and go to cause negative slips.

In fact, the nanostructured surface is roughened as well. Based on the continuum assumption, the microflow field in microchannels with uniformly distributed rough elements was analyzed by Hu and co-workers [55]. They found that the pressure drop was greatly increased by the existence of the surface roughness for low Reynolds number flow through microchannels. The fluid dynamical effects were attributed to two factors: causing the expansion and compression of the streamlines, and obstructing the flow directly. The nanoscale flow fields of the liquid flow in the roughened nanochannels obtained by our molecular dynamics simulations are presented in Fig. 7. In the mainstream regimes, the streamlines are essentially the same as those in smooth channels, which indicates the liquid flows in the middle of the nanochannels are not disturbed by the presence of the surface nanoroughness. Adjacent to the nanostructured surface about one time of the nanogeometry size, the liquid streamlines expand between two nanostructure units and then compress above the structure peaks periodically. Beneath the largest part of the diastemata between the roughness units, the liquid has no macroscopic velocity along the flow direction. Thus, beneath the nanostructure diastemata are dead zones, which indicate a direct obstruction of the liquid nanoflow by the roughness units. The streamline distortion and the backwater block unquestionably imply additional drag. In other words, the apparent boundary slip should be reduced. The near-wall streamlines for the hydrophilic liquid-wall interaction with $c=1.0$ shown in Fig. 7(a) are distorted more profoundly than those for the hydrophobic interaction with $c=0.4$ shown in Fig. 7(b). It indicates that the nanostructure block to the liquid nanoflows for the hydrophilic liquid-solid interaction is stronger than that for the hydrophobic liquid-solid interaction.

Generally, the nanostructure effects on the surface wettability and the near-surface streamlines are simultaneous, which is accordingly called a dual effect. The surface hydrophilicity can be enhanced or weakened by the nanostructures depending on the liquid-wall interactions. It is noticeable that the nanostructure surface may even show superhydrophobicity for the liquid-wall hydrophobic interaction and enlarge the boundary slip of the liquid nanoflows. However, the near-surface streamlines are meanwhile distorted and blocked by the roughness effect of the surface nanostructures, which often causes the apparent slip decrease. Consequently, the dual effect of the surface nanostructures leads to a nonmonotonic dependence of the slip length on the nanostructure size, which implies that the surface nanostructures can be applied to control the friction of liquid micro- and nanoflows.

IV. CONCLUSION

We consider liquid wetting and flow in surface-nanostructured nanochannels by molecular dynamics simulations. The results show that the dependence of the slip length and friction for the liquid nanoflow on the nanostructure size is exactly nonmonotonic. This is demonstrated to arise from a dual effect of the surface nanostructures, i.e., simultaneous effects on the surface wettability and the hydrodynamic disturbance. On the one hand, the surface nanostructures can result in homogeneous(heterogeneous) fluid organizations in the vicinity of the surface for the hydrophilic(hydrophobic) liquid-solid interactions, which enhances the surface wettability described by the Cassie and Wenzel models. For the hydrophobic liquid-wall interaction, especially, the nanostructured surface may even show superhydrophobicity due to a nanoscale lotus effect, which often leads to very large boundary velocity slip for the liquid flow. On the other hand, the nanostructures distort the nanoscale streamlines of the liquid flow near the channel surfaces and block the nanoflow directly, which decreases the apparent slip length equivalently. The dual effect implies that surface nanostructuring may offer a promising opportunity to control the friction of liquid micro- and nanoflows.

ACKNOWLEDGMENT

This work is financially supported by National Natural Science Foundation of China (Grant No. 10372051).

[1] C. M. Ho and Y. C. Tai, Annu. Rev. Fluid Mech. **30**, 579 (1998).
[2] H. G. Craighead, Science **290**, 1532 (2000).
[3] N. Giordano and J. T. Cheng, J. Phys.: Condens. Matter **13**, R271 (2001).
[4] Z. Y. Guo and Z. X. Li, Int. J. Heat Mass Transfer **46**, 149 (2003).
[5] M. Gad-el-Hak, Phys. Fluids **17**, 100612 (2005).
[6] T. M. Squires and S. R. Quake, Rev. Mod. Phys. **77**, 977 (2005).
[7] F. M. White, *Fluids Mechanics* (McGraw-Hill, New York, 2003).
[8] K. Watanabe, Yanuar, and H. Udagawa, J. Fluid Mech. **381**, 225 (1999).
[9] R. Pit, H. Hervet, and L. Leger, Phys. Rev. Lett. **85**, 980 (2000).
[10] J. Baudry, E. Charlaix, A. Tonck, and D. Mazuyer, Langmuir **17**, 5232 (2001).
[11] D. C. Tretheway and C. D. Meinhart, Phys. Fluids **14**, L9 (2002).
[12] Y. Zhu and S. Granick, Phys. Rev. Lett. **88**, 106102 (2002).
[13] C. H. Choi, K. J. A. Westin, and K. S. Breuer, Phys. Fluids **15**, 2897 (2003).
[14] C. Cottin-Bizonne, B. Cross, A. Steinberger, and E. Charlaix, Phys. Rev. Lett. **94**, 056102 (2005).
[15] P. Joseph and P. Tabeling, Phys. Rev. E **71**, 035303(R) (2005).
[16] L. Joly, C. Ybert, and L. Bocquet, Phys. Rev. Lett. **96**, 046101 (2006).
[17] C. Neto, D. R. Evans, E. Bonaccurso, H. J. Butt, and V. S. J. Craig, Rep. Prog. Phys. **68**, 2859 (2005).
[18] P. A. Thompson and M. O. Robbins, Phys. Rev. A **41**, 6830 (1990).
[19] M. Sun and C. Ebner, Phys. Rev. Lett. **69**, 3491 (1992).
[20] J. Koplik and J. R. Banavar, Annu. Rev. Fluid Mech. **27**, 257 (1995).
[21] J. L. Barrat and L. Bocquet, Phys. Rev. Lett. **82**, 4671 (1999).
[22] M. Cieplak, J. Koplik, and J. R. Banavar, Phys. Rev. Lett. **86**, 803 (2001).
[23] G. Nagayama and P. Cheng, Int. J. Heat Mass Transfer **47**, 501 (2004).
[24] S. C. Hendy, M. Jasperse, and J. Burnell, Phys. Rev. E **72**, 016303 (2005).
[25] R. S. Voronov, D. V. Papavassiliou, and L. L. Lee, J. Chem. Phys. **124**, 204701 (2006).
[26] W. Barthlott and C. Neinhuis, Planta **202**, 1 (1997).
[27] X. F. Gao and L. Jiang, Nature (London) **432**, 36 (2004).
[28] E. Bonaccurso, M. Kappl, and H. J. Butt, Phys. Rev. Lett. **88**, 076103 (2002).
[29] J. Ou, B. Perot, and J. P. Rothstein, Phys. Fluids **16**, 4635 (2004).
[30] S. Gogte, P. Vorobieff, R. Truesdell, A. Mammoli, F. Swol, P. Shah, and C. J. Brinker, Phys. Fluids **17**, 051701 (2005).
[31] C. H. Choi and C. J. Kim, Phys. Rev. Lett. **96**, 066001 (2006).
[32] C. H. Choi, U. Ulmanella, J. Kim, C. M. Ho, and C. J. Kim, Phys. Fluids **18**, 087105 (2006).
[33] R. Truesdell, A. Mammoli, P. Vorobieff, F. van Swol, and C. J. Brinker, Phys. Rev. Lett. **97**, 044504 (2006).
[34] J. Davies, D. Maynes, B. W. Webb, and B. Woolford, Phys. Fluids **18**, 087110 (2006).
[35] B. Y. Cao, M. Chen, and Z. Y. Guo, Chem. J. Chin. Univ. **26**, 277 (2005).
[36] M. Cieplak, J. Koplik, and J. R. Banavar, Phys. Rev. Lett. **96**, 114502 (2006).
[37] A. Jabbarzadeh, J. D. Atkinson, and R. I. Tanner, Phys. Rev. E **61**, 690 (2000).
[38] S. C. Yang and L. B. Fang, Mol. Simul. **31**, 971 (2005).
[39] K. M. Jansons, Phys. Fluids **31**, 15 (1988).
[40] K. Sarkar and A. Prosperetti, J. Fluid Mech. **316**, 223 (1996).
[41] I. V. Ponomarev and A. E. Meyerovich, Phys. Rev. E **67**, 026302 (2003).
[42] T. M. Galea and P. Attard, Langmuir **20**, 3477 (2004).
[43] N. V. Priezjev, A. A. Darhuber, and S. M. Troian, Phys. Rev. E **71**, 041608 (2005).
[44] O. I. Vinogradova and G. E. Yakubov, Phys. Rev. E **73**, 045302(R) (2006).
[45] R. S. Voronov, D. V. Papavassiliou, and L. L. Lee, J. Chem. Phys. **124**, 204701 (2006).
[46] B. Y. Cao, M. Chen, and Z. Y. Guo, Appl. Phys. Lett. **86**, 091905 (2005).
[47] S. Maruyama and T. Kimura, in Proceedings of the 5th ASME-JSME Thermal Engineering Joint Conference, San Diego, USA, 1999.
[48] P. A. Thompson and S. M. Troian, Nature (London) **389**, 360 (1997).
[49] M. P. Allen and D. J. Tildesley, *Computer Simulation of Liquids* (Oxford University, New York, 1989).
[50] G. S. Grest and K. Kremer, Phys. Rev. A **33**, 3628 (1986).
[51] P. G. de Gennes, Rev. Mod. Phys. **57**, 827 (1985).
[52] A. B. D. Cassie and S. Baxter, Trans. Faraday Soc. **40**, 546 (1944).
[53] R. N. Wenzel, Ind. Eng. Chem. **28**, 988 (1936).
[54] X. D. Wang, X. F. Peng, J. F. Lu, T. Liu, and P. X. Wang, J. Therm. Sci. **2**, 230 (2003).
[55] Y. D. Hu, C. Werner, and D. Q. Li, ASME J. Fluids Eng. **125**, 871 (2003).